Study of the Refraction Effects in Microwave Breast Imaging Using a Dry Setup *

Daniela M. Godinho, João M. Felício, *Member, IEEE*, Carlos A. Fernandes, *Senior Member, IEEE*, and Raquel C. Conceição

***Abstract*—Medical Microwave Imaging (MWI) has been studied as a technique to aid breast cancer diagnosis. Several different prototypes have been proposed but most of them require the use of a coupling medium between the antennas and the breast, in order to reduce skin backscattering and avoid refraction effects. The use of dry setups has been addressed and recent publications show promising results. In this paper, we assess the importance of considering refraction effects in the image reconstruction algorithms. To this end, we consider a simplified homogeneous spherical model of the breast and analytically compute the propagating rays through the air-body interface. The comparison of results considering only direct ray propagation or refracted rays shows negligible impact on the accuracy of the images for moderately high permittivity media. Thus, we may avoid the computational burden of calculating the refracted rays in complex shapes.**

***Clinical Relevance*—Microwave Imaging (MWI) is a low-cost emerging imaging technique to aid breast cancer diagnosis. The study of refraction effects in MWI is relevant to design a prototype which simultaneously implies low maintenance burden and is capable of providing an image reconstruction in almost real time with reduced computational cost.**

I. Introduction

Breast cancer is the second most common cancer worldwide, with approximately 2.09 million new cancer cases in 2018 [1]. The currently used imaging techniques to aid breast cancer diagnosis are X-ray mammography, ultrasound, Magnetic Resonance Imaging (MRI), and Computed Tomography (CT). These technologies have their own disadvantages, including the use of ionising radiation, user-dependency or high cost. Microwave Imaging (MWI) has been studied as a complementary imaging screening technique since it presents advantages such as the use of non-ionising radiation and low power and the fact it does not require breast compression and may potentially be user-independent and very low-cost.

One of the techniques often used for MWI is Ultra-Wide Band radar (UWB) which consists in transmitting very short impulse signals into the breast using one or more antennas and recording the backscattered signals. These scattered signals are firstly processed using artefact removal algorithms to remove the strong skin backscattering, followed by imaging algorithms to create a reflectivity profile of the breast.

Several microwave breast imaging prototypes have been proposed in the last few decades, mostly varying on the number and/or configuration of antennas and the type of system – monostatic, when only one antenna transmits and receives, or multistatic when one antenna transmits and the remaining record the backscattering. Most of the presented prototypes require the immersion of the breast in a coupling liquid [2-5] in order to reduce the reflection on the breast surface. However, the immersion medium attenuates the transmitted signals [6], poses sanitation issues and makes the examination unpractical.

Some works have presented "air-operated" alternatives by incorporating the antennas in a bra and putting them in contact with the breast skin [7]. Moreover, our research group has assessed the feasibility of using a dry imaging setup [8], where the single antenna sweeps the breast in a cylindrical configuration. We experimentally demonstrated that the tumour scattered signals are not excessively affected by the contrast between air/skin interface, as long as the breast shape is accurately retrieved and a suitable artefact removal algorithm is used [8]. Currently, we are evaluating the viability of using a focal lens in a multistatic system to enhance the energy coupling into the breast, and thus overcome the absence of immersion liquid [9].

Although we have extensively studied the impact of not using an immersion liquid to reduce reflection at the skin/air interface, it remains to be assessed how relevant are refraction effects on the imaging results. In this paper, we analyse the relevance of refraction effects on an "air-operated system". To this end, we assume a spherical homogeneous breast, in order to avoid the computationally heavy calculations of the refracted rays. Moreover, the simplified shape allows an analytical closed form to calculate the refracted ray paths. Despite this geometry simplification, the study provides important clues on whether refraction is relevant for path length calculations involved in the imaging algorithm.

*Research supported by Fundação para a Ciência e a Tecnologia-FCT under the fellowship SFRH/BD/129230/2017, FCT/MEC (PIDDAC) under the Strategic Programme UIDB/BIO/00645/2020, and also by FCT/MEC through national funds, and by FEDER–PT2020 Partnership Agreement under Grant UID/EEA/50008/2019.

D. M. Godinho, and R. C. Conceição are with Instituto de Biofísica e Engenharia Biomédica, Faculdade de Ciências da Universidade de Lisboa, 1749-016 Lisbon, Portugal (corresponding author: dgodinho94@gmail.com; raquelcruzconceicao@gmail.com).

J. M. Felício is with Centro de Investigação Naval (CINAV), Escola Naval, Almada, Portugal, and with Instituto de Telecomunicações, Instituto Superior Técnico, Universidade de Lisboa, Lisbon, Portugal (e-mail: joao.felicio@lx.it.pt).

C. A. Fernandes is with Instituto de Telecomunicações, Instituto Superior Técnico, Universidade de Lisboa, Lisbon, Portugal (e-mail: carlos.fernandes@lx.it.pt).

II. Setup under investigation

In this section, we present the numerical setup and the antenna used to conduct the present study. All elements were designed and simulated using Computer Simulation Technology (CST) Microwave Studio software [10].

A. Setup

For the purpose of this study, the breast is represented as a 50 mm radius homogeneous dielectric sphere, Fig. 1. Two targets are embedded in the phantom at x = 30 mm and x = - 30 mm (y = 0 mm and z = 0 mm) and simulated as Perfect Electric Conductors (PEC) spheres of 5 mm radius. The numerical breast phantom is characterised by a relative permittivity $\varepsilon_r = 8$ and a loss tangent of 0.1, which corresponds approximately to the upper limit of fat permittivity [11]. A realistic breast is not homogeneous, but the proposed model is sufficient to represent the breast in proof-of-concept studies as shown in [8], avoiding additional confounders. It is noted that many reconstruction algorithms consider a homogenous media with average uniform permittivity. Also, the used permittivity value represents the average permittivity of the region underneath the skin where refraction can be more significant.

We consider only monostatic signals collected by twelve antennas circularly distributed in the *xy*-plane around the breast phantom, at 80 mm radius and 30° step, as shown in Fig. 1. The gap between the dielectric surface and the antenna in the *xy*-plane is thus 30 mm.

B. Antenna

We use a planar slot-based single-layer printed antenna formed by two crossed exponential slots (in short, XETS). The antenna presents a balanced structure and is fed between two metallisation "petals" [12]. Its main advantages include a very pure linear polarisation along the entire bandwidth, a stable radiation pattern and phase centre. The XETS used for this study has 28 mm radius (Fig. 2) and is impedance-matched from 2 to 6 GHz (Fig. 3).

III. Signal processing

This section briefly addresses the signal processing algorithms: image reconstruction and analytical calculation of refracted rays. In both formulations, we assume that the antenna radiates a spherical wave, although it operates in the near-field regime.

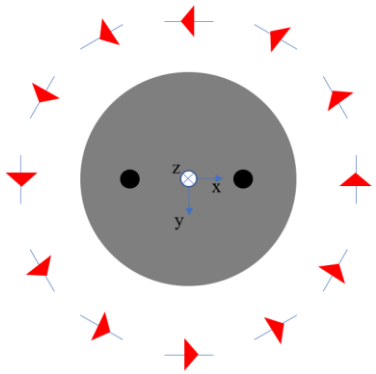

Fig. 1. Monostatic setup considered in this study. The grey circle represents the dielectric sphere, the black circles represent the targets and each blue line and red arrow represents an antenna and the respective polarisation orientation.

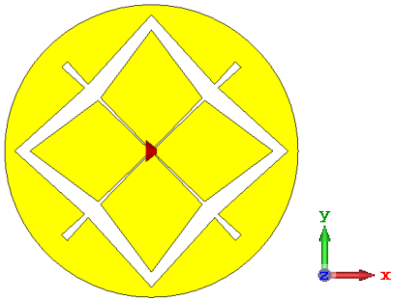

Fig. 2. XETS antenna layout used in this study.

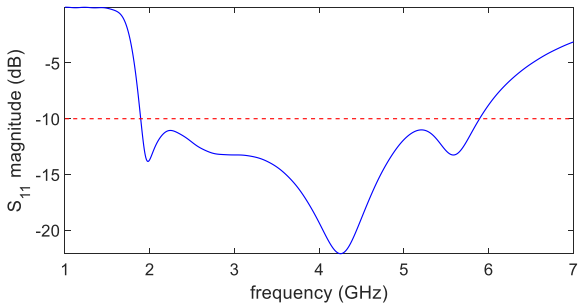

Fig. 3. Plot of the magnitude in dB of the input reflection coefficient (s_{11}) of the XETS antenna over frequency.

A. Imaging reconstruction algorithm

We use an image reconstruction algorithm based on wave migration algorithm [13], which is very robust and yields similar results to other commonly used algorithms, such as Delay-and-Sum [14, 15]. The intensity at any voxel in the volume is calculated accounting for the distances between each antenna position and that voxel:

$$intensity(v) = \sum_{i}^{N_a} \sum_{f_k}^{N_f} s_{ii}(f_k)\, e^{2jk_0 (d_{air} + n_{diel}\, d_{diel})} \quad (1)$$

where d_{air} is the distance between each XETS and the entry point on the sphere, including the electric length of the XETS [16], d_{diel} is the distance from the entry point to voxel *v*, and n_{diel} is the dielectric refractive index, N_a is the number of antennas, s_{ii} is the $1 \times N_f$ array with the scattering parameter measured by the i^{th} antenna position after removing the skin backscattering, N_f is the number of frequency points, and $k_0 = 2\pi f(f_k)/c$ is the free-space wavenumber at frequency f_k with c as the speed of light in vacuum. Fig. 4 illustrates the geometry for the raypaths with and without refraction. It is assumed that the antenna phase centre is well-known and stable.

An "ideal" calibration is considered at this stage, in order to remove the response from the skin. In other words, the term $s_{ii}(f_k)$ in (1) is calculated as the difference of the reflection coefficient with and without PEC targets. This avoids additional confounders and focuses solely on the response of the targets.

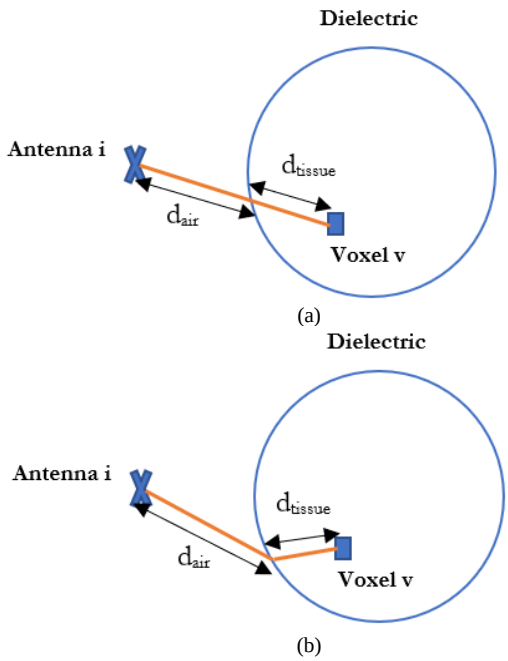

Fig. 4. Schematic of the distances used in the image reconstruction algorithm for a case where refraction effects (a) are not and (b) are considered.

B. *Refraction algorithm*

The refraction effects are calculated using Snell law in vector form [17]:

$$\left(\frac{1}{\sqrt{\varepsilon_r}}\hat{\imath} - \hat{t}\right) \times \hat{N} = 0 \tag{2}$$

where $\hat{\imath}$ is the unit vector in the incident direction, $\hat{N}$ is the unit normal vector inside the sphere, $\hat{t}$ is the unit vector in the direction of the refracted ray, and ε_r is the relative permittivity value of the dielectric sphere. Given the voxel coordinates and the antenna position coordinates, Eq, (2) lends an analytical solution for the ray entry point coordinates in the sphere. Although multiple solutions are sometimes found, the correct solution can be singled-out using physical arguments. The calculated entry points are used in the imaging algorithm to compute d_{air} and d_{diel}, considering the whole 3D volume.

IV. Results

The radar signal $s_{ii}(f_k)$ in eq. (1) is obtained by full wave simulation of the proposed geometry. The corresponding reconstructed images in *xz* and *xy* planes not considering refraction (only direct ray propagation) are presented in Fig. 5 for $\varepsilon_r = 8$. The magnitude of the reflected signals is represented in a colour map, where the lighter colors correspond to higher intensities. The targets are well detected, corresponding to their true location represented with the red dashed circles. The images lack resolution in the *xz*-plane because the antennas are distributed only in a single *xy*-plane.

As a comparison, in Fig. 6 we present the reconstructed images for the same permittivity values but now accounting for the refraction effects, also in *xz* and *xy* planes. The targets are just as easily identified, compared to the scenarios in Fig. 5. There is a slight difference in the magnitude values that corresponds to a better focusing when refraction is taken into account in the calculations. This is not surprising. However, there is no significant improvement in the imaging results when considering refraction. Consequently, we conclude that there is no significant advantage in taking the burden of calculating the refracted rays in the tested scenario, in an air-operated setup like ours.

V. Conclusions

In this paper we studied the refraction effects on a MWI monostatic setup with no immersion liquid. The incident and refracted rays were calculated using an analytical formulation which is only possible due to the regular geometry of the phantom. In non-uniform shapes like the breast or the head, the calculation of refraction may have a very high computational cost.

The results show no significant improvement when refraction is taken into account in the calculations in the scenario where a spherical breast with $\varepsilon_r = 8$ (i.e., low-density breast) is considered, thus allowing to conclude that the refraction is mostly irrelevant in the presented setups for image reconstruction. This encourages the use of MWI dry setup since it does not require additional increase of computational cost. We will investigate the refraction effects in models with different shapes, higher permittivity values and while considering heterogeneity in future work.

References

[1] International Agency for Research on Cancer - World Health Organization, "GLOBOCAN 2018: Estimated Cancer Incidence, Mortality and Prevalence Worldwide in 2018 - Cancer Fact Sheets," 2018. [Online]. Available: http://gco.iarc.fr/today/fact-sheets-cancers

[2] P. M. Meaney, M. W. Fanning, D. Li, S. P. Poplack, and K. D. Paulsen, "A Clinical Prototype for Active Microwave Imaging of the Breast", *IEEE Transactions on Microwave Theory and Techniques*, 48(11), pp. 1841-1853, 2000.

[3] E. C. Fear et al., "Microwave breast imaging with a monostatic radar-based system: A study of application to patients", *IEEE Transactions on Microwave Theory and Techniques*, 61(5), pp. 2119-2128, 2013.

[4] A. W. Preece, I. Craddock, M. Shere, L. Jones, and H. L. Winton, "MARIA M4: clinical evaluation of a prototype ultrawideband radar scanner for breast cancer detection", *Journal of Medical Imaging*, 3(3), pp. 2016.

[5] A. Fasoula et al., "On-Site Validation of a Microwave Breast Imaging System, before First Patient Study", *Diagnostics*, 8(3), pp. 1-38, 2018.

[6] N. K. Nikolova, "Microwave imaging for breast cancer", *IEEE Microwave Magazine*, 12(7), pp. 78-94, 2011.

[7] A. Santorelli, E. Porter, S. Dantas, M. Popović, and J. Schwartz, "Low-cost hardware for a time-domain microwave system for breast health monitoring," EuCAP, Davos, Switzerland. 1-4, 2016.

[8] J. M. Felício, J. M. Bioucas-Dias, J. R. Costa, and C. A. Fernandes, "Microwave Breast Imaging using a Dry Setup", *IEEE Transactions on Computational Imaging*, (in press), pp. 1-15, 2019.

[9] D. M. Godinho, J. M. Felício, C. A. Fernandes, and R. C. Conceicao, "Feasibility study of focal lens for multistatic microwave breast imaging," ICECOM, Dubrovnik, Croatia, (in press), 2019.

[10] "CST – Computer Simulation Technology." [Online]. Available: https://www.cst.com/

[11] M. Lazebnik et al., "A Large-Scale Study of the Ultrawideband Microwave Dielectric Properties of Normal, Benign and Malignant Breast Tissues Obtained from Cancer Surgeries", *Physics in Medicine and Biology*, 52, pp. 6093–6115, 2007.

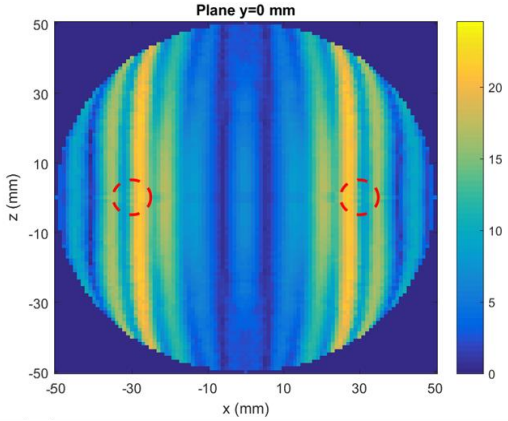

(a)

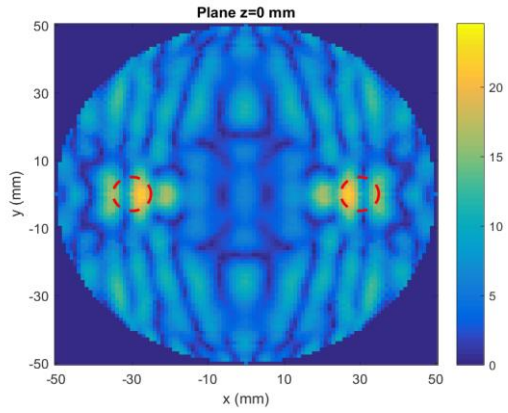

(b)

Fig. 5. Reconstructed images without considering refraction on a dielectric sphere with $\varepsilon_r = 8$ and two targets inside. Both *xz* and *xy* planes are represented in (a) and (b), respectively. The actual location and shape of the targets is represented as red dashed circles.

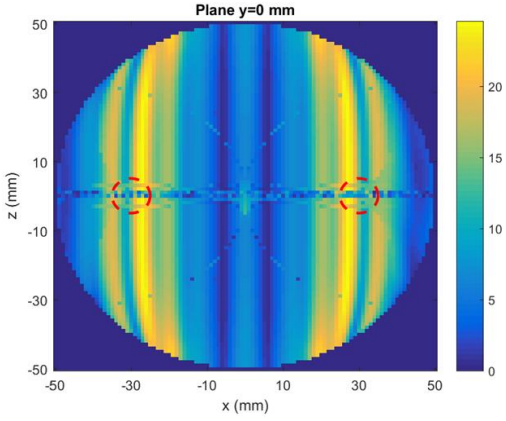

(a)

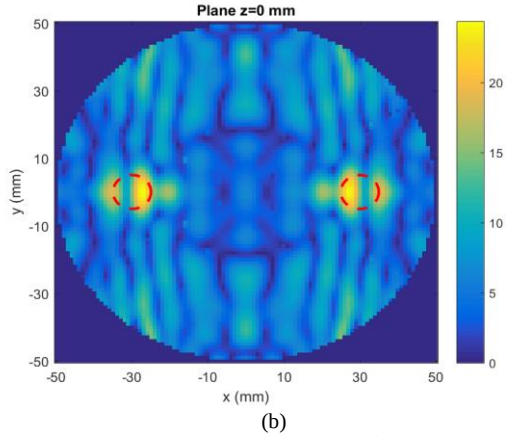

(b)

Fig. 6. Reconstructed images considering refraction on a dielectric sphere with $\varepsilon_r = 8$ and two targets inside. Both *xz* and *xy* planes are represented in (a) and (b), respectively. The actual location and shape of the targets is represented as red dashed circles.

[12] J. R. Costa and C. A. Fernandes, "Broadband slot feed for integrated lens antennas", *IEEE Antennas and Wireless Propagation Letters*, 6, pp. 2007.

[13] J. M. Lopez-Sanchez and J. Fortuny-Guasch, "3-D Radar Imaging Using Range Migration Techniques", *IEEE Transactions on Antennas and Propagation*, 48(5), pp. 728-737, 2000.

[14] R. Benjamin, "Synthetic, post-reception focusing in near-field radar," Synthetic, post-reception focusing in near-field radar, Edinburgh, UK: IET, 1996.

[15] E. C. Fear, X. Li, S. C. Hagness, and M. A. Stuchly, "Confocal Microwave Imaging for Breast Cancer Detection: Localization of Tumors in Three Dimensions", *IEEE Transactions on Biomedical Engineering*, 49(8), pp. 812-822, 2002.

[16] J. M. Felício, J. M. Bioucas-Dias, J. R. Costa, and C. A. Fernandes, "Antenna Design and Near-Field Characterization for Medical Microwave Imaging Applications", *IEEE Transactions on Antennas and Propagation*, 67(7), pp. 4811-4824, 2019.

[17] C. A. Fernandes, J. R. Costa, and E. B. Lima, "Dielectric Lens Antennas," in *Handbook of Antenna Technologies*, Z. N. Chen, Ed. 1 ed. Singapore: Springer, 2016.